Universal Scaling of the Figure of Merit of Plasmonic Sensors

Peter Offermans,[†] Martijn C. Schaafsma,[‡] Said R. K. Rodriguez,[‡] Yichen Zhang,[‡] Mercedes Crego-Calama,[†] Sywert H. Brongersma,[†] and Jaime Gómez Rivas[‡,§,*]

[†]Holst Centre/imec-nl, High Tech Campus 31, 5656 AE Eindhoven, The Netherlands, [‡]Center for Nanophotonics, FOM Institute AMOLF, c/o Philips Research Laboratories, High Tech Campus 4, 5656 AE Eindhoven, The Netherlands, and [§]Department of Applied Physics, Eindhoven University of Technology, P.O. Box 513, NL-5600 MB Eindhoven, The Netherlands

Metallic nanoparticles are the object of intensive research as they exhibit a characteristic optical response governed by the excitation of localized surface plasmon resonances (LSPRs). These resonances are the result of the coherent oscillation of the free electrons in the metallic particle driven by an electromagnetic field. Because of the sensitivity of LSPRs to the medium surrounding the nanoparticle, they are of interest for the development of sensitive biochemical sensors employing ultrasmall detection volumes. The figure of merit (FoM) of plasmonic sensors is commonly defined as the resonance shift upon a change in the refractive index of the surrounding dielectric normalized by the resonance line width. Narrow resonances improve thus the FoM of plasmonic sensors. Recently, a direct experimental comparison between the refractive index sensing capabilities of LSPRs in gold nanoparticles and propagating surface plasmon polaritons on extended gold surfaces or surface plasmon resonances (SPRs) was presented.[1] Despite offering a low bulk refractive index sensing figure of merit (FoM) of typically 1−2, it was found that LSPR-based sensing is a highly competitive technique to conventional SPR for the detection of changes in the refractive index close to the surface. This high sensitivity has been attributed to the large confinement of the LSPR electromagnetic field around the nanostructures.[1] Further improvements in the FoM of gold nanoparticle sensors have been recently introduced by coupling plasmonic resonances in structures of two or more nanoparticles,[2−5] nanoholes,[6] and nanowells.[7] This coupling can lead to narrow Fano resonances[8] that result from the interference between a discrete state (resonantly scattered light) and a continuum of states (nonresonant scattering).[9]

ABSTRACT We demonstrate an improvement by more than 1 order of magnitude of the figure of merit (FoM) of plasmonic nanoparticle sensors by means of the diffractive coupling of localized surface plasmon resonances. The coupling in arrays of nanoparticles leads to Fano resonances with narrow line widths known as surface lattice resonances, which are very suitable for the sensitive detection of small changes in the refractive index of the surroundings. We focus on the sensitivity to the bulk refractive index and find that the sensor FoM scales solely with the frequency difference between the surface lattice resonance and the diffracted order grazing to the surface of the array. This result, which can be extended to other systems with coupled resonances, enables the design of plasmonic sensors with a high FoM over broad spectral ranges with unprecedented accuracy.

KEYWORDS: plasmon · sensing · resonance · figure-of-merit · nanoparticle · scaling

In this article, we demonstrate the enhanced sensitivity of Fano resonances in periodic arrays of metallic particles to minute changes in the refractive index of the surrounding medium. In particular, we show an improvement of the FoM by more than 1 order of magnitude compared to that of LSPRs by coupling these localized resonances with Rayleigh anomalies. Rayleigh anomalies represent the onset of diffraction in a grating. At the wavelength and angle of incidence corresponding to the Rayleigh anomaly, there is a transition between a diffracted order propagating in the plane of the array and an evanescent diffracted order. At this wavelength and angle, the wave vector of the diffracted order is parallel to the surface of the array enhancing the coupling of the LSPRs. This coupling leads to the appearance of narrow resonances in the transmittance and reflectance spectra of the array. These resonances are known as surface lattice resonances and were first proposed by Carron et al. in the context of surface-enhanced Raman scattering.[10] In subsequent works this idea was further developed by Schatz and co-workers.[11] The first experimental indications of this phenomenon were observed in 1D arrays.[12]
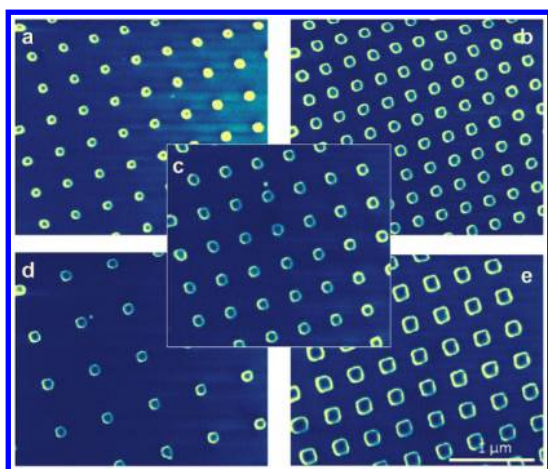
Figure 1. SEM images of gold nanoparticles arrays on quartz with varying particle diameter and lattice constants: (a) 95 nm diameter, lattice constant 400 nm; (b) 110 nm diameter, lattice constant 300 nm; (c) 110 nm diameter, lattice constant 400 nm; (d) 110 nm diameter, lattice constant 600 nm; (e) 165 nm diameter, lattice constant 400 nm.

Only very recently, has there been clear demonstration of the excitation of these modes in arrays of small particles and nanoantennas,[13−18] and the first demonstration of the use of these resonances for optical sensing have been presented.[19] Within the framework of Fano resonances, surface lattice resonances can be described as the interference between a broad localized surface plasmon resonance due to radiation damping and a narrow resonance given by the Rayleigh anomaly. This interference gives rise to the asymmetric line shapes characteristic for Fano resonances.[8]

Furthermore, we find that the FoM for arrays of low loss metals, that is, metals with an imaginary component of the permittivity much smaller than the modulus of the real component, is ultimately governed by the frequency difference between the surface lattice resonance and the Rayleigh anomaly. This frequency difference is controlled by the lattice constant of the array and the dimensions of the particles. Such a universal scaling of the FoM does not exist in disordered arrays of nanoparticles, which do not exhibit collective behavior.[1,20] As the spectral position of the surface lattice resonances is determined by geometrical parameters,[18] they offer huge flexibility in the design of the response of plasmonic sensors.

RESULTS AND DISCUSSION

Several arrays of gold nanoparticles with a height of 50 nm were fabricated on top of a quartz substrate by e-beam lithography and ion-milling. The dimensions of the arrays are $100 \times 100 \ \mu m^2$. The gold nanoparticles were designed with a diameter of 95, 110, 145, and 165 nm, the lattice structure is square with a lattice constant of a = 300, 350, 400, 450, 500, 550, and 600 nm. A scanning electron microscope image of some of the arrays is shown in Figure 1.
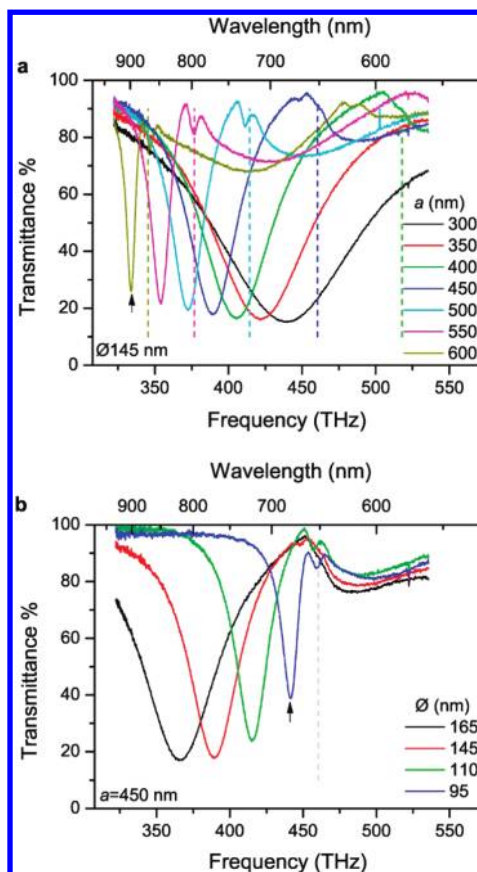
Figure 2. Transmittance spectra of gold nanoparticle arrays. (a) Spectra of gold nanoparticle arrays on quartz embedded in a liquid environment with n = 1.45 as function of frequency for different lattice constants a = 300, 350, 400, 450, 500, 550, and 600 nm. The average particle size was 145 nm $\times$ 145 nm $\times$ 50 nm. (b) Spectra of gold nanoparticle arrays on quartz embedded in a liquid environment with n = 1.45 as function of frequency for different average particle diameters d = 95, 110, 145, and 165 nm. The lattice constant a and height were 450 and 50 nm, respectively. The vertical lines in panels a and b correspond to the frequency of the Rayleigh anomaly $\nu_{RA} = c/(na)$.

To illustrate the effect of diffractive coupling in periodic arrays of nanoparticles, Figure 2a shows the transmittance spectra at normal incidence for arrays with lattice constant in the range of 300−600 nm, embedded in a symmetric environment with refractive index n = 1.45. This symmetric environment is achieved by exposing the nanoantenna array to a liquid with the same refractive index as the silica substrate. The spectra show strong dips reaching transmittance values of less than 20%. These resonances redshift and narrow considerably with increasing lattice constant. The vertical lines in the figure indicate the wavelength of the diffraction edges $\nu_{RA} = c/(na)$, with c being the speed of light in vacuum. These frequencies represent the Rayleigh anomaly conditions at which the $(\pm 1, 0)$ and $(0, \pm 1)$ diffracted orders become evanescent for normal incidence. Note that the dips in transmittance occur on the low-frequency side of the corresponding Rayleigh anomaly. This is a characteristic feature of

surface lattice modes, which arise from the coupling of surface plasmon polaritons localized at each nanoparticle site to the Rayleigh anomaly.[14] The eigenfrequencies of these lattice modes correspond to the frequencies that give rise to poles in the effective polarizability of the array. In the coupled-dipole approximation for an infinite array,[21,22] the effective polarizability is expressed as

$$\alpha^* = \frac{1}{1/\alpha - S} \qquad (1)$$

where α is the polarizability of the individual particles and S is the retarded dipole sum, which accounts for the contribution of the scattered field by the array to α^*. It can been shown that, with increasing lattice constant, both the real and the imaginary part of S become more negative, leading to a redshift of ν_{SLR} and a narrowing of the lattice resonances by partial cancellation of the damping.[22] This behavior explains the trend observed in Figure 2a.

The position and width of surface lattice resonances do not only depend on the lattice constant, but also on particle diameter. Figure 2b shows the transmittance spectra at normal incidence for different average particle diameters d = 95, 110, 145, and 165 nm, with a lattice constant of 450 nm. The resonances blueshift with decreasing particle diameter and narrow as their resonance wavelength approaches that of the Rayleigh anomaly, indicated by the vertical dashed line. Note that for the surface lattice resonances indicated by the arrows in Figure 2a and Figure 2b, the frequency difference between the Rayleigh anomaly and the surface lattice resonance, $\nu_{RA} - \nu_{SLR}$, and the resonance width are very similar. These similarities are striking given the very large differences in particle diameter and lattice constant. As will be shown below, it is possible to define a scaling parameter $\delta = (\nu_{RA} - \nu_{SLR})/\nu_{RA}$ that solely defines the figure of merit (FoM) of sensors based on surface lattice resonances. This parameter provides a measure of the coupling strength of the localized surface plasmon resonance to the Rayleigh anomaly. An important consequence of this universal scaling is that by tuning both the lattice constant and particle diameter such that δ remains constant, it is possible to shift surface lattice resonances over a wide spectral range without affecting their width and FoM. This behavior is a major advantage for sensing applications as it enables the use of narrow resonances at specific predefined wavelengths.

The sensing performance of plasmonic structures can be characterized by the figure of merit FoM = $S_{bulk}/\Delta\lambda$, where $\Delta\lambda$ is the resonance width and S_{bulk} is the bulk sensitivity defined as $S_{bulk} = \partial\lambda/\partial n$, that is, the shift of the resonance wavelength upon a change of the refractive index of the surrounding medium n. Narrow resonances are advantageous for sensing applications as they enable an accurate determination of the
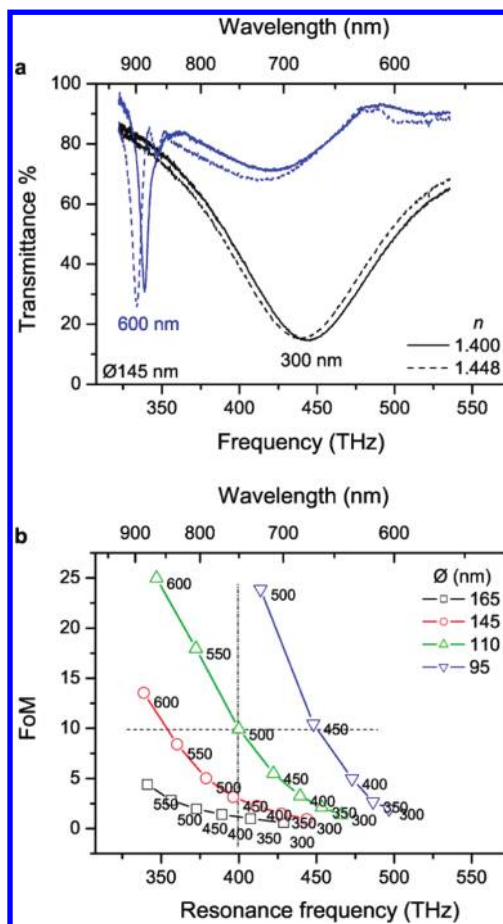
Figure 3. Transmittance spectra and FoM for different gold nanoparticle arrays. (a) Transmittance spectra for two gold nanoparticle arrays with lattice constant a = 300 nm and a = 600 nm on quartz embedded in a liquid environment with n = 1.40 (solid lines) and n = 1.45 (dashed lines) as function of frequency. Particle diameter and height are 145 and 50 nm, respectively. (b) Figure of merit for particle arrays with diameters 95 (down triangles), 110 (up triangles), 145 (circles), 165 (squares) nm, height 50 nm and lattice constant a = 300, 350, 400, 450, 500, 550, and 600 nm as indicated in the legend, as function of surface lattice resonance frequency. The horizontal dashed line indicates that the resonance frequency can be tuned over a large range with the same FoM, by varying the particle diameter and lattice constant. The vertical dash-dotted line indicates that the FoM can be increased for a fixed resonance frequency by tuning both particle diameter and lattice constant.

resonance shift upon changes in the environment by monitoring the transmittance at a wavelength close to resonance. This advantage is illustrated in Figure 3a where we compare the transmittance spectra of particle arrays with a lattice constant of 300 and 600 nm for n = 1.40 (solid lines) and for n = 1.45 (dashed lines). Upon changing the refractive index of the environment, the resonances redshift due to a modification of the coupling condition between the incident plane wave and the surface lattice resonance. This shift results in an increased transmittance at the initial resonance frequency. The array with a lattice constant of 300 nm is characterized by a broad lattice resonance
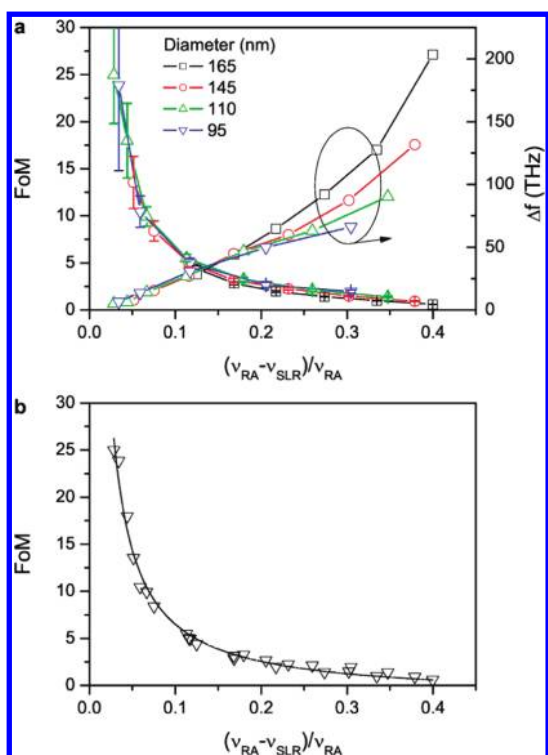
Figure 4. Measured FoM for different gold nanoparticle arrays and fit of the experimental data. (a) Experimental FoM $(\partial\lambda/\partial n)/\Delta\lambda$ and the full width at half-maximum Δf of surface lattice resonances as a function of the parameter $\delta = (v_{RA} - v_{SLR})/v_{RA}$ for particle arrays with diameters 95, 110, 145, and 165 nm, height 50 nm, and lattice constant a = 300, 350, 400, 450, 500, 550, and 600 nm. (b) The solid line is a fit to the experimental data (symbols) indicating a reciprocal scaling of the FoM with δ.

Figure 5. Calculated FoM for gold (squares), silver (dots), and copper (triangles) nanoparticle arrays with diameters 95, 110, 145, 165 nm, height 50 nm and lattice constant a = 300, 350, 400, 450, 500, 550, and 600 nm as function of $\delta = (v_{RA} - v_{SLR})/v_{RA}$. The solid line is a fit to the data with FoM = $1.2/\delta$.

with a bulk sensitivity comparable to that of LSPRs found in disordered arrays of nanoparticles.[1] The transmittance in this sample increases only few percent when the refractive index is varied. In contrast, the array with a lattice constant of 600 nm shows a surface lattice resonance that is narrower by an order of magnitude with a bulk sensitivity that is almost 2 times higher, which results in an increased transmittance at the resonance frequency by more than 40% when the refractive index is varied from 1.40 to 1.45. As the electromagnetic field of surface lattice modes can extend up to several tens to hundreds of nanometers out of the plane of the array[16] they are ideally suited for bulk sensing applications such as vapor/gas detection with thick (porous) sensing layers[23] or the detection of large (bio)molecules, such as proteins.[24] It has been shown that a reduction of the surface lattice resonance line width (leading to a larger FoM) is also related to a longer decay length of the field out of the plane of the array.[16] Therefore, for the detection of small molecules close to the particle array, there will be a trade-off in sensitivity between a reduction of the line width and a weaker field confinement.

We plot the experimental FoM as a function of the surface lattice resonance frequency for nanoparticle arrays with different diameter and lattice constants in

Figure 3b. The FoM increases strongly as the lattice constant increases and as the diameter of the particles decreases from a value of about 1−2 for arrays with small lattice constant and large diameter, to values as high as 25 for arrays with large lattice constant and small diameter. This large increase of the FoM by more than 1 order of magnitude stresses the relevance of coupled plasmonic resonances for optical sensing. As indicated in Figure 3b by the horizontal dashed line, the resonance frequency can be tuned over a wide range while maintaining a constant FoM. This behavior can be achieved by varying particle diameter and lattice constant. The FoM can be increased at a fixed resonance frequency, by tuning both particle diameter and the lattice constant (vertical dash-dotted line, Figure 3b).

As noted above, the width of the resonances is related to the difference between the resonance frequency and the frequency of the Rayleigh anomaly $v_{RA} - v_{SLR}$. To investigate this dependency further, we plot both the FoM of the resonances and their full width at half-maximum Δf in Figure 4a as function of the dimensionless parameter $\delta = (v_{RA} - v_{SLR})/v_{RA}$, which measures the detuning of lattice resonances from the Rayleigh anomaly. Interestingly, we find that all the measurements collapse to a single curve despite the large variations in lattice constant and particle diameter. The increase in the FoM at smaller δ is paired with a decreasing Δf, while at larger δ an increasing spread in Δf can be observed. For clarity, we repeat the same measurements of the FoM as a function of δ in Figure 4b. The solid curve indicates the empirical dependence of the FoM with δ, namely,

$$\text{FoM} = \frac{0.79}{\delta} - 1.38 \qquad (2)$$

With a small offset, the FoM varies thus with $1/\delta$.

To confirm this behavior of the FoM, we have performed calculations of the transmission spectra using a model based on the coupled dipole approximation. In this model, the particles are assumed to be oblate spheroids with only a dipolar polarizability, surrounded

by a homogeneous environment. The polarizabilities are obtained from the modified long wavelength approximation.[25] The calculation was performed for gold nanoparticle arrays consisting of 30 particles × 30 particles. The permittivity of gold was taken from ref 26. The results of the calculations, represented with squares in Figure 5, are in qualitative agreement with the experimental data shown in Figure 4. This is a remarkable result regarding the relatively large size of the particles from which we can expect a significant multipolar contribution to the scattering of light. The good agreement between measurements and calculations considering only dipolar contributions to the scattering allows us to state that this dipolar scattering dominates the optical response of the sample. The universal scaling of the FoM with δ pertains not only to gold nanoparticles, but also to other noble metal nanoparticles. Figure 5 shows calculations for Au (squares), Ag (dots), and Cu (triangles). Within the numerical error of the calculations, we find that the FoM scales similarly for the different materials. In general, we can state that the FoM scales inversely with δ as long as the Ohmic losses in the metal are small, that is, as long as the imaginary component of the permittivity of the metal is much smaller that the modulus of the real component. Calculations done for lossy metals (not shown here), for example, Ni, confirm this behavior.

The universal scaling of the FoM with the dimensionless parameter $\delta = (v_{RA} - v_{SLR})/v_{RA}$ is rooted in the dependence of the surface lattice resonance line width on its detuning from the Rayleigh anomaly. This fundamental principle can be understood in light of an analogy with a simple model consisting of two linearly coupled harmonic oscillators.[27−30] The first oscillator represents the conduction electrons in the metallic nanoparticles, upon which acts a harmonic driving force $F = F_0 e^{-i2\pi vt}$ representing the optical excitation. The second oscillator represents the Rayleigh anomaly, that is, an electromagnetic field grazing to the surface of the array. The equations of motion for such a system are

$$\ddot{x}_1 + \gamma_1 \dot{x}_1 + v_1^2 x_1 - \Omega_{12}^2 x_2 = F_0 e^{-i2\pi vt}$$
$$\ddot{x}_2 + \gamma_2 \dot{x}_2 + v_2^2 x_2 - \Omega_{12}^2 x_1 = 0 \qquad (3)$$

where x_i, γ_i, and v_i ($i = 1, 2$) are the displacement from equilibrium position, damping, and eigenfrequency of the ith oscillator, respectively. Ω_{12} is the coupling frequency between the two oscillators and represents the interaction strength between the nanoparticles in the array and the Rayleigh anomaly.

Since we are interested in the extinct optical power due to the oscillation of the conduction electrons in the nanoparticles, we calculate the absorbed mechanical power by oscillator 1 from the driving force F, $P(t) = F\dot{x}$. Integrating $P(t)$ over one period of oscillation and scanning the driving frequency v yields the absorbed power spectrum $A(v)$. The quantity $1 - A$ is grossly proportional to the transmittance, given that $1 - T = E$, with T being
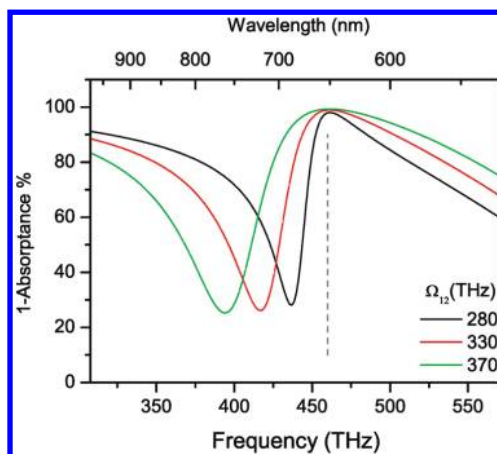
Figure 6. Calculation of the absorbed power spectrum of two coupled oscillators. The absorbed power spectrum was calculated for three different coupling frequencies $\Omega_{12} =$ 280 (black), 330 (red), and 370 (green) THz.

the transmittance and E being the extinction. Figure 6 shows calculations of $1 - A$ for three coupling frequencies: $\Omega_{12} = 280$, 330, and 370 THz. All other parameters in the model are fixed for the three cases at $F_0 = 7$ ms^{-2}, $\gamma_1 = 400$ THz, $\gamma_2 = 2$ THz, $v_1 = 700$ THz, $v_2 = v_{RA} = 460$ THz. Note that we use F_0 as a fitting parameter determining the amplitude of the calculated spectra. This allows a qualitative comparison between the resonance line shapes for the three coupling frequencies as this value, together with the dampings and eigenfrequencies, is kept constant for all three cases.

The eigenfrequency of the second oscillator v_2, is indicated by the vertical dashed line in Figure 6. The resonance dips at slightly lower frequencies than v_2 arise from the coupling of oscillator 1 to oscillator 2. A comparison of Figure 6 with Figure 2b shows that just as the coupling of the nanoparticles to diffracted orders leads to surface lattice resonances at slightly lower frequencies than the Rayleigh anomaly, the coupling of oscillator 1 to oscillator 2 leads to a resonance at slightly lower frequencies than the eigenfrequency v_2. The central finding of this analogy is the connection between the coupling frequency, Ω_{12}, and the characteristics of the resonances. Namely, as Ω_{12} increases, the detuning $v_{RA} - v_{SLR}$ increases and the resonance line width broadens. Thus, the detuning provides a measure of the coupling strength of the nanoparticles to the Rayleigh anomaly. Note that although the damping constants are equal in all the three calculations of Figure 6—not likely to be the case in the experiment since the particle size changes and therefore Ohmic and radiative losses change—the line width is strongly affected by the detuning of the resonance from v_2. As a consequence, the FoM, which is inversely proportional to the line width, scales also with the detuning $v_{RA} - v_{SLR}$. We therefore see in a simple manner how the universal scaling law previously discussed has its origins in the

radiative coupling strength of nanoparticles to diffracted orders. Furthermore, this result clarifies the previously mentioned similarity between the two resonances indicated by the arrows in Figure 2 panels a and b; that is, despite the differences in particle size and lattice constants, both resonances have similar line shapes because the coupling strength between the particles and the corresponding Rayleigh anomalies are very similar in both cases. We should point out that the analogy between the array of nanoantennas and the simple coupled oscillator model indicates that a similar scaling behavior can be expected for other plasmonic sensors based on Fano resonances.[31,32]

CONCLUSION

To summarize, we have demonstrated that surface lattice resonances in ordered arrays of gold nanoparticles offer a sensing performance that is at least an order of magnitude better than that of localized plasmon resonances associated with disordered particle arrays. These lattice resonances can be tuned over a wide spectral range by tuning both the lattice constant of the array and the diameter of the particles. We find that the sensor FoM is ultimately governed by the frequency difference between the surface lattice resonance and the Rayleigh anomaly of the array. This universal scaling, which is valid for metals with low Ohmic losses, has been reproduced with calculations based on arrays of coupled dipoles and has been explained using a simple coupled-oscillator model. The analogy between arrays of nanoparticles and the coupled-oscillator model indicates that a similar scaling behavior of the FoM can be expected in other systems exhibiting coupled plasmonic resonances.

METHODS

Transmittance spectra were obtained by illuminating the sample with a collimated beam of unpolarized light from a halogen lamp at normal incidence. The transmission was measured through the arrays and normalized to the transmission through the quartz substrate. Bulk refractive index sensitivity measurements were performed by flowing liquids with different refractive index (Cargille Laboratories) in the range $n = 1.40$ to 1.45 over the substrate by means of a flow cell. Choosing a refractive index of the liquid close to that of the substrate allows an efficient diffractive coupling between the nanoparticles in a (nearly) homogeneous dielectric environment.[18]

REFERENCES AND NOTES

1. Svedendahl, M.; Chen, S.; Dmitriev, A.; Käll, M. Refractometric Sensing Using Propagating *versus* Localized Surface Plasmons: A Direct Comparison. *Nano Lett.* **2009**, *9*, 4428–4433.
2. Enoch, S.; Quidant, R.; Badenes, G. Optical Sensing Based on Plasmon Coupling in Nanoparticle Arrays. *Opt. Express* **2004**, *12*, 3422–3427.
3. Sonnefraud, Y.; Verellen, N.; Sobhani, H.; Vandenbosch, G. A.; Moshchalkov, V. V.; Dorpe, P. V.; Nordlander, P.; Maier, S. A. Experimental Realization of Subradiant, Superradiant, and Fano Resonances in Ring/Disk Plasmonic Nanocavities. *ACS Nano* **2010**, *4*, 1664–1670.
4. Lassiter, J. B.; Sobhani, H.; Fan, J. A.; Kundun, J.; Capasso, F.; Nordlander, P.; Halas, N. J. Fano Resonances in Plasmonic Nanoclusters: Geometrical and Chemical Tunability. *Nano Lett.* **2010**, *10*, 3184–3189.
5. Hao, F.; Sonnefraud, Y.; Dorpe, P. V.; Maier, S. A.; Halas, N. J.; Nordlander, P. Symmetry Breaking in Plasmonic Nanocavities: Subradiant LSPR Sensing and a Tunable Fano Resonance. *Nano Lett.* **2008**, *8*, 3983–3988.
6. Henzie, J.; Lee, M.; Odom, T. Multiscale Patterning of Plasmonic Metamaterials. *Nat. Nanotechnol.* **2007**, *2*, 549–554.
7. Hicks, E. M.; Zhang, X.; Zou, S.; Lyandres, O.; Spears, K. G.; Schatz, G. C.; Van Duyne, R. P. Plasmonic Properties of Film over Nanowell Surfaces Fabricated by Nanosphere Lithography. *J. Phys. Chem. B* **2005**, *109*, 22351–22358.
8. Fano, U. Effects of Configuration Interaction on Intensities and Phase Shifts. *Phys. Rev.* **1961**, *124*, 1866–1878.
9. Genet, C.; Van Exter, M. P.; Woerdman, J. P. Fano-Type Interpretation of Red Shifts and Red Tails in Hole Array Transmission Spectra. *Opt. Commun.* **2003**, *225*, 331–336.
10. Carron, K. T.; Fluhr, W; Meier, M.; Wokaun, A.; Lehmann, H. W. Resonances of Two-Dimensional Particle Gratings in Surface-Enhanced Raman Scattering. *J. Opt. Soc. Am. B* **1986**, *3*, 430–440.
11. Zou, S.; Schatz, G. Narrow Plasmonic/Photonic Extinction and Scattering Line Shapes for One and Two Dimensional Silver Nanoparticle Arrays. *J. Chem. Phys.* **2004**, *121*, 12606–12.
12. Hicks, E.; Zou, S.; Schatz, G.; Spears, K.; Van Duyne, R.; Gunnarsson, L.; Rindzevicius, T.; Kasemo, B.; Käll, M. Controlling Plasmon Line Shapes Through Diffractive Coupling in Linear Arrays of Cylindrical Nanoparticles Fabricated by Electron Beam Lithography. *Nano Lett.* **2005**, *5*, 1065–1070.
13. Kravets, V. G.; Schedin, F.; Kabashin, A. V.; Grigorenko, A. N. Extremely Narrow Plasmon Resonances Based on Diffraction Coupling of Localized Plasmons in Arrays of Metallic Nanoparticles. *Phys. Rev. Lett.* **2008**, *101*, 087403–6.
14. Auguié, B.; Barnes, W. Collective Resonances in Gold Nanoparticle Arrays. *Phys. Rev. Lett.* **2008**, *101*, 143902–5.
15. Chu, Y.; Schonbrun, E.; Yang, T.; Crozier, K. Experimental Observation of Narrow Surface Plasmon Resonances in Gold Nanoparticle Arrays. *Appl. Phys. Lett.* **2009**, *93*, 181108–10.
16. Vecchi, G.; Giannini, V.; Gómez Rivas, J. Shaping the Fluorescent Emission by Lattice Resonances in Plasmonic Crystals of Nanoantennas. *Phys. Rev. Lett.* **2009**, *102*, 146807–10.
17. Vecchi, G.; Giannini, V.; Gómez Rivas, J. Surface Modes in Plasmonic Crystals Induced by Diffractive Coupling of Nanoantennas. *Phys. Rev. B* **2009**, *80*, 201401–4.
18. Auguié, B.; Bendaña, X. M.; Barnes, W. L.; García de Abajo, F. J. Diffractive Arrays of Gold Nanoparticles Near an Interface: Critical Role of the Substrate. *Phys. Rev. B* **2010**, *82*, 155447–13.
19. Kravets, V. G.; Schedin, F.; Kabashin, A. V.; Grigorenko, A. N. Sensitivity of Collective Plasmon Modes of Gold Nanoresonators to Local Environment. *Opt. Lett.* **2010**, *35*, 956–958.
20. Miller, M.; Lazarides, A. Sensitivity of Metal Nanoparticle Surface Plasmon Resonance to the Dielectric Environment. *J. Phys. Chem. B* **2005**, *109*, 21556–21565.
21. Zou, S.; Janel, N.; Schatz, G. C. Silver Nanoparticle Array Structures that Produce Remarkably Narrow Plasmon Lineshapes. *J. Chem. Phys.* **2004**, *120*, 10871–5.

22. Haynes, C. L.; McFarland, A. D.; Zhao, L.; Van Duyne, R. P.; Schatz, G. C.; Gunnarsson, L.; Prikulis, J.; Kasemo, B.; Käll, M. Nanoparticle Optics: The Importance of Radiative Dipole Coupling in Two-Dimensional Nanoparticle Arrays. *J. Phys. Chem. B* **2003**, *107*, 7337–7342.

23. Podgorsek, R. P.; Franke, H. Selective Optical Detection of Aromatic Vapors. *Appl. Opt.* **2002**, *41*, 601–608.

24. Green, R. J.; Frazier, R. A.; Shakesheff, K. M.; Davies, M. C.; Roberts, C. J.; Tendler, S. J. B. Surface Plasmon Resonance Analysis of Dynamic Biological Interactions with Biomaterials. *Biomaterials* **2000**, *21*, 1823–1835.

25. Kelly, K. L.; Coronado, E.; Zhao, L. L.; Schatz, G. C. The Optical Properties of Metal Nanoparticles: The Influence of the Size, Shape and Dielectric Environment. *J. Phys. Chem. B.* **2003**, *107*, 668–677.

26. Palik, E. D. *Handbook of Optical Constants of Solids III*; Academic Press: Boston, MA, 1998.

27. Alzar, C.; Martinez, M.; Nussenzveig, P. Classical Analog of Electromagnetically Induced Transparency. *Am. J. Phys.* **2002**, *70*, 37–41.

28. Hao, F.; Nordlander, P.; Sonnefraud, Y.; Dorpe, P. V.; Maier, S. A. Tunability of Subradiant Dipolar and Fano-Type Plasmon Resonances in Metallic Ring/Disk Cavities: Implications for Nanoscale Optical Sensing. *ACS Nano* **2009**, *3*, 643–652.

29. Mukherjee, S.; Sobhani, H.; Lassiter, J. B.; Bardhan, R.; Nordlander, P.; Halas, N. J. Fanoshells: Nanoparticles with Built-in Fano Resonances. *Nano Lett.* **2010**, *10*, 2694–2701.

30. Liu, N.; Langguth, L.; Weiss, T.; Kastel, J.; Fleischhauer, M.; Pfau, T.; Giessen, H. Plasmonic Analogue of Electromagnetically Induced Transparency at the Drude Damping Limit. *Nat. Mater.* **2009**, *8*, 758–762.

31. Miroshnichenko, A. E.; Flach, S.; Kivshar, Y. S. Fano Resonances in Nanoscale Structures. *Rev. Mod. Phys.* **2010**, *82*, 2257–2298.

32. Luk'yanchuk, B.; Zheludev, N. I.; Maier, S. A.; Halas, N. J.; Nordlander, P.; Giessen, H.; Chong, C. T. The Fano Resonance in Plasmonic Nanostructures and Metamaterials. *Nat. Mater.* **2010**, *9*, 707–715.